Letter

Analytical solution of inertia effect in high-speed flows through disordered porous media

Zhiguo Tian, Yunfan Huang, and Moran Wang*
Department of Engineering Mechanics, Tsinghua University, Beijing 100084, China

(Received 15 March 2024; accepted 8 October 2024; published 28 October 2024)

We present an analytical solution of flow through disordered porous media with inertia effects at a finite Reynolds number (Re), and consequently a truncated quadratic formula for easy use without any fitting parameters. The derivation is based on an effective capillary model in which the effective radius of capillaries varies with Re. Inspired by the asymptotic solution of flow in curved capillaries [S. Murata, Y. Miyake, and T. Inaba, J. Fluid Mech. **73**, 735 (1976)], the Oseen-form equation is derived to capture the flow behavior in each capillary. The analytical formula has been validated by comparisons with numerous available experimental data.

DOI: 10.1103/PhysRevFluids.9.L102101

Introduction. High-speed single-phase flows in disordered porous media are commonly encountered in various engineering applications [1–5]. The quadratic equation, $-\mathrm{d}p/\mathrm{d}x = \alpha q + \beta q^2$, with α and β as parameters, known as the Forchheimer equation or Ergun equation [6,7], incorporates a quadratic term into the classical Darcy's law. It has been widely used as an empirical correlation to capture the relationship between the pressure gradient, $-\mathrm{d}p/\mathrm{d}x$, and the Darcy velocity, q, for high-speed flows in permeable media. However the physics of this quadratic formula has not been well understood yet. For decades, the quadratic term had been ascribed to occurrence of turbulence, since Reynolds' contribution in 1901 [8]. Consequently, more and more reliable experiments for flows in porous media [9] have demonstrated that the quadratic equation is able to capture the flow behavior within a wider range of Re even before turbulence fully developed, which has been comprehensively discussed in [10]. To date, a well-accepted physical explanation for the quadratic term is a general inertia effect rather than turbulence only and it has been well acknowledged that the classical Navier-Stokes equations is the starting point for deriving the quadratic form equation.

Various modeling strategies have been adopted to derive formal solutions, such as the simple-structure abstraction method [11,12], the asymptotic expansion method [13–15], and the volume averaging method [16–23]. In the simple-structure abstraction method, orders of magnitude analyses were conducted on each term of the Navier-Stokes equations, assuming the internal structures as sphere arrays or other simple geometries, to derive a formal solution with undetermined parameters. The asymptotic expansion method, by assuming the inner structure of porous media as periodic ones and the characteristic length of periodic cells much smaller than the entire domain, simplified the Navier-Stokes equation as a series of linearized equations, and thus acquired the tensorial formal solution [13–15]. In the volume averaging method, properties of porous structure and fluid were averaged in a representative elementary volume (REV) level, while requiring additional closure hypotheses to obtain formal solutions. These methods have been working well generally, except meeting challenges in special effects in porous media such as inertia effect, slipping effects [24–27], and fluid adsorption [28] on solid surfaces.

*Contact author: mrwang@tsinghua.edu.cn

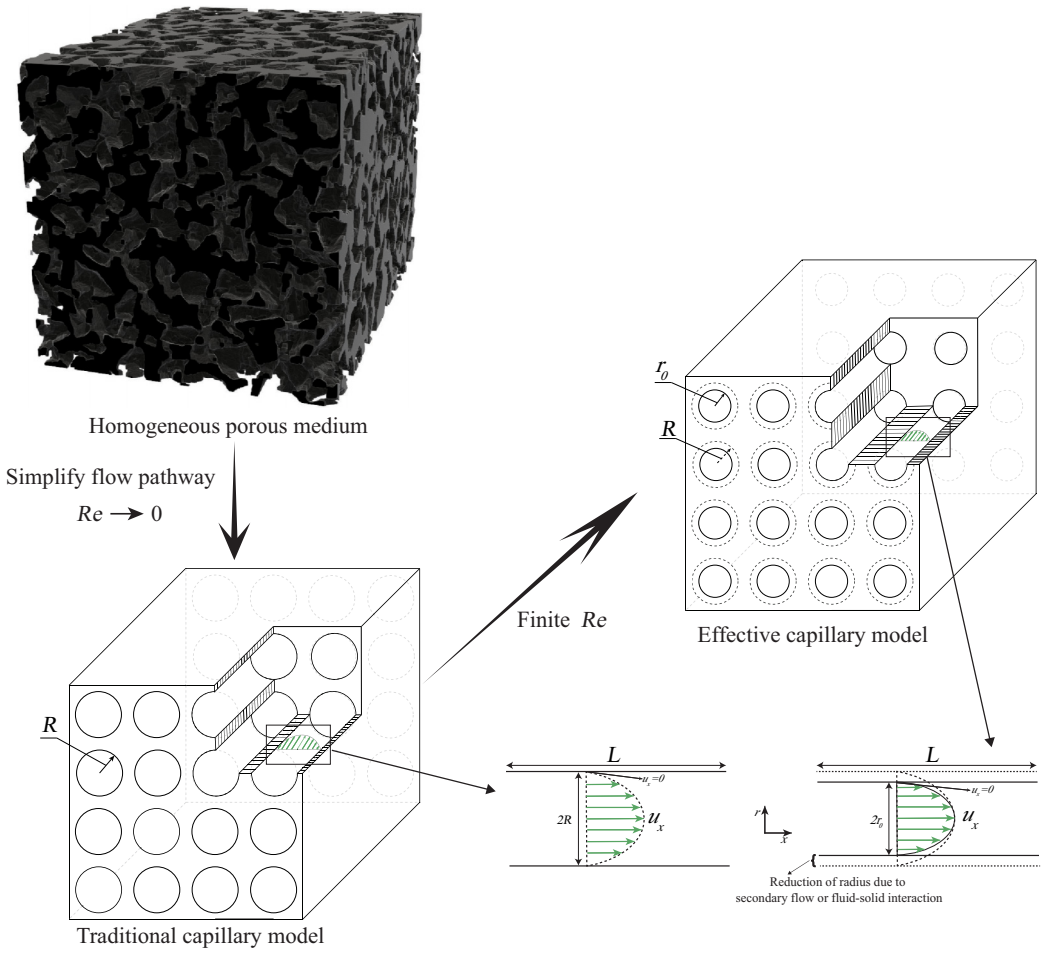

FIG. 1. The diagram of the developed capillary model. The tortuous flow pathways in complex geometries of porous media are simplified as a bundle of parallel straight capillaries in the traditional capillary model. R is the effective radius of the capillaries. The traditional capillary model bridges the Stokes flow with the Darcy's flow at a very low Re. For a finite value of Re, the effective capillary model proposes a reduced effective radius r_0 due to secondary flows near solid surfaces to reflect the intensity of inertia effect.

To describe the inertia effects accurately, one has to capture the effects from both complex geometries of porous media and complicated behavior of high-speed flows, as well as the exact values of formula parameters. Recent numerical studies have provided important information of flow fields and transition mechanism from Darcy's flows to inertial flows [1–3,10,29–31], however, an analytical description of inertial flows is still absent. It is noticed that the permeability of sphere packs at a low Reynolds number [32–35] or a low but finite Reynolds number [13] can be analytically determined without knowledge of numerical simulations. It is reasonable to expect an analytical solution, and further an empirical formula for engineering applications, of inertia effect in high-speed flows through disordered porous media.

Physical and mathematical models.

a. Physical model and governing equations. The capillary model, in which the flow pathways of fluid in porous media are modelled as a bundle of evenly arranged straight capillaries, is a simplified model for theoretical analysis [36], as shown in Fig. 1. The traditional capillary model

has an effective capillary radius, R, to recover the equivalent flow resistance through the complex geometries of porous media. With a nonslip boundary condition at surfaces, this model can bridge the Stokes flow with the classical Darcy's flow at a very low Re [36]. It was also successful in derivation of Klinkenberg formula by assigning a slip boundary condition on surfaces at high Knudsen numbers [37]. However, application of this capillary model to capture the inertia effect for high-speed flows is not straightforward since the analytical solution of Poiseuille flow in a capillary is always the same for an either high or low Re. Therefore, a new model is necessary to capture the inertia effect through capillaries.

To capture the disordered effect of complex geometry of porous media on flow, we notice that the previous analyses by asymptotic perturbation of the laminar flow in a curved pipe [38–41] have proven that as long as the curvature radius $\mathcal{R}$ of the pipe is much larger than its cross-sectional radius R, the streamwise velocity is $u_x = R^2\Delta P[1-(r/R)^2]/(4\mu L) + \mathcal{O}(R/\mathcal{R})$, the radial direction velocity is $u_r = R^2\Delta P(\mathrm{Re}/288)[1-(r/R)^2]^2[4-(r/R)^2] \times \sin\theta/(4\mu \mathrm{L}) + \mathcal{O}((\mathrm{R}/\mathcal{R})^2)$ and the azimuthal velocity is $u_\theta = R^2\Delta P(\mathrm{Re}/288)[1-(r/R)^2][7(r/R)^4 - 23(r/R)^2 + 4] \times \cos\theta/(4\mu \mathrm{L}) + \mathcal{O}((\mathrm{R}/\mathcal{R})^2)$. Here, ΔP is the pressure difference, L is the length of the pipe, μ is the dynamic viscosity of the fluid, Re is the Reynolds number of a Poiseuille flow in a capillary defined as $\mathrm{Re} = \frac{(\Delta P)R^2}{4\mu L}\frac{R}{\nu}$, and θ is the polar angle. It is easy to find that the streamwise velocity depends only on the position, r, whose value reaches the maximum in the central of the capillary $u_x|_{r=0}$ and is always equal to the maximum velocity of a Poiseuille flow in a straight capillary driven by the same pressure gradient, and the radial direction velocity caused by secondary flows increases with Re.

Therefore, we develop further an effective capillary model for flows in disordered porous media at a finite Re, as shown in Fig. 1. The secondary flows caused by inertia effects raise the flow resistance and therefore lead to a reduction of effective radius of capillaries. For a steady-state and fully developed flow in the effective capillaries, the streamwise momentum equation can be written as: $u_r\frac{\partial u_x}{\partial r} = -\frac{1}{\rho}\frac{\mathrm{d}p}{\mathrm{d}x} + \nu(\frac{\partial^2 u_x}{\partial r^2} + \frac{1}{r}\frac{\partial u_x}{\partial r})$, where $\frac{\mathrm{d}p}{\mathrm{d}x}$ is assumed constant. It should be noted that this equation may not be valid for highly heterogeneous porous media. Radius distribution rather than uniform radius can be assigned to represent possible heterogeneity of samples for further improvement of accuracy. Furthermore, u_r can be decomposed into $u_r(r,\theta) = U_r + \widetilde{u_r}(r,\theta)$. U_r is the average value over the cross section which should be zero due to the polar angle θ ranges from 0 to 2π, and $\widetilde{u_r}(r,\theta)$ is the fluctuation part. The fluctuation part can be assumed to be proportional to the average streamwise velocity over the cross section of one single capillary, U_x, $\widetilde{u_r}(r,\theta) = M(r,\theta)\cdot U_x$, where $M(r,\theta)$ is a proportional coefficient, as a common formal closure hypothesis in the volume average method [10,22]. This indicates that u_r is proportional to U_x. Therefore, without losing generality, we preserve the average streamwise velocity caused by inertia effects and assume M to be irrelevant with r,θ and Re, simply noting MU_x as U, and thus the governing equation is linearized as follows in the cylindrical coordinate system:

$$U\frac{\mathrm{d}u}{\mathrm{d}r} = -\frac{1}{\rho}\frac{\mathrm{d}p}{\mathrm{d}x} + \nu\left(\frac{\mathrm{d}^2u}{\mathrm{d}r^2} + \frac{1}{r}\frac{\mathrm{d}u}{\mathrm{d}r}\right), \tag{1}$$

where U is the averaged streamwise velocity over the cross section of the capillary caused by inertia effects, u, $\frac{\mathrm{d}p}{\mathrm{d}x}$ are the velocity and the pressure gradient in the streamwise direction, respectively, and r, x are the radial and streamwise coordinate, respectively. Note that U should be a function of Re and disorder degree of microstructure of porous media. It is also interesting to find that Eq. (1) has a very similar mathematical form as the Oseen equation [42]. The classical Oseen equation focuses on external flows, while Eq. (1) derived in this work is to capture the inertia effects in the capillaries.

b. Analytical solution and parameter determinations. Equation (1) is a second-order ordinary differential equation and the theoretical solution can be obtained by integral as

$$u = C_1\int_0^{r^*}\frac{e^{r^*}}{r^*}\mathrm{d}r^* + \frac{\nu^2}{U^2}\frac{1}{\mu}\frac{\mathrm{d}p}{\mathrm{d}x}[-r^* - \ln r^* - \gamma + \mathrm{Ei}(r^*)] + C_2, \tag{2}$$

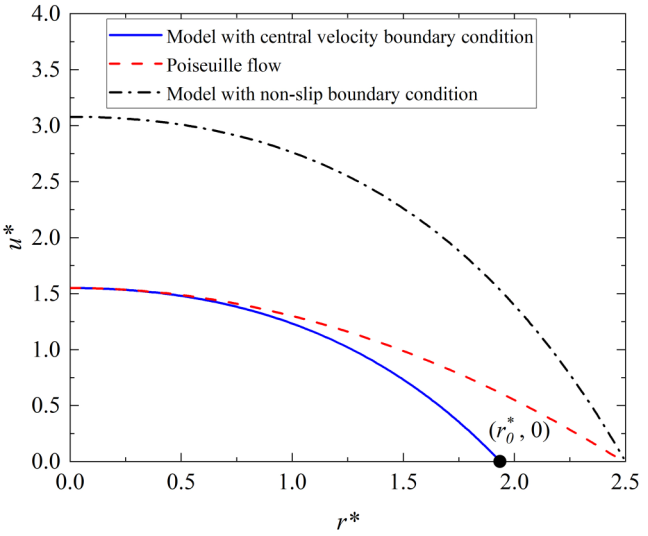

FIG. 2. Comparison of dimensionless velocity profiles determined by different boundary conditions at $\mathrm{Re}_R = 2.5$. Result with the nonslip boundary condition [Eq. (5)] overestimates the velocity compared with the Poiseuille flow [$u^* = (\mathrm{Re}_R^2 - r^{*2})/4$]. Implementation of the central velocity boundary condition [formula (6)] gives reasonable velocity profile [formula] and the radius is posteriorly truncated. r_0 is the effective tube radius which is defined by Eq. (8) in our effective capillary model and $r_0^* = Ur_0/\nu$ is the dimensionless position.

where $\mathrm{Ei}(r^*) = \int_{-\infty}^{r^*} \frac{e^{r^*}}{r^*} \mathrm{d}r^*$ is the exponential integral, and $\gamma = 0.5772\ldots$ is the Euler's constant which originates from $\lim_{x\to 0} \mathrm{Ei}(x) - \lim_{x\to 0} \ln(x) = \gamma$ because of the property of the exponential integral Ei(x). $r^* = Ur/\nu$ is the dimensionless position defined by the local position r in the straight capillaries, and C_1, C_2 are two constants to be determined by the boundary conditions.

Following a standard solution of the Poiseuille flow, the nonslip boundary condition and a limited value of velocity at the central line can be used:

$$u|_{r=R} = 0, \tag{3}$$

$$u|_{r=0} \neq \infty, \tag{4}$$

which lead to a parameter determination of Eq. (2) as

$$u_{\mathrm{non-slip}} = -\frac{\nu^2}{U^2}\frac{1}{\mu}\frac{\mathrm{d}p}{\mathrm{d}x}[r^* + \ln r^* - \mathrm{Ei}(r^*) - \mathrm{Re}_R - \ln \mathrm{Re}_R + \mathrm{Ei}(\mathrm{Re}_R)], \tag{5}$$

where $\mathrm{Re}_R = UR/\nu$ is the Reynolds number defined by U in the capillary. Figure 2 shows the comparison of the velocity profiles between Eq. (5), illustrated as the black dash-dotted line, and the solution of a Poiseuille flow, as the red dashed line, driven by the same pressure gradient. As Fig. 2 shows, the velocity profile of Eq. (5) is much higher than that of the Poiseuille flow, which is practically impossible because the inertia effects caused by secondary flows in curved flow pathway can only increase the resistance and therefore reduce the flow rate through the capillaries in contrast to the Poiseuille flow driven by the same pressure gradient.

Inspired by the previous study on flows in curved pipes [38–40], we adopt the central-velocity boundary condition which means that the velocity at the central of a capillary equals to the central (maximum) velocity of the Poiseuille flow driven by the same pressure gradient, with an accuracy

of $\mathcal{O}(R/\mathcal{R})$:

$$u|_{r=0} = -\frac{v^2}{U^2}\frac{1}{\mu}\frac{\mathrm{d}p}{\mathrm{d}x}\frac{{\mathrm{Re}_R}^2}{4}. \tag{6}$$

Combining the governing Eq. (1) with the boundary condition, Eq. (6), the analytical solution can be obtained as

$$u^* = \frac{u}{-\frac{v^2}{U^2}\frac{1}{\mu}\frac{\mathrm{d}p}{\mathrm{d}x}} = r^* + \ln r^* + \gamma - \mathrm{Ei}(r^*) + \frac{{\mathrm{Re}_R}^2}{4}. \tag{7}$$

A new velocity profile calculated by Eq. (7) has been added in Fig. 2, as the blue solid line shows, for a comprehensive comparison with the previous two profiles. As can be seen that the velocity reaches to zero earlier to the wall position of capillary (r_0), which means that the secondary flow near walls at a finite Re reduces the flow rate indeed. This analysis is very consistent with the proposed effective capillary model in Fig. 1. Here, we define the effective capillary radius, r_0, by letting $u|_{r=r_0} = 0$ in Eq. (7) and solve it out if needed:

$$r_0^* + \ln r_0^* + \gamma - \mathrm{Ei}(r_0^*) + \frac{{\mathrm{Re}_R}^2}{4} = 0. \tag{8}$$

The intensity of the inertia effect is related to the reduction of the effective tube radius r_0 compared with R. Here, we highlight two insights regarding the effective capillary model: (1) The flow rates measured by experiments are lower than prediction of the Darcy's law in high-speed flow in porous media [9,43–45]; (2) The inertia effects caused by the secondary flows near walls are ascribed to the reduction of flow rate. By the derived governing equations based on the effective capillary model and the central-velocity boundary condition, we can analytically capture the flow rate reduction in experiments at finite Re's.

To calculate the effective permeability of porous media with inertia effects, the volumetric flow rate of capillaries Q_{eff} can be obtained by

$$\begin{aligned} Q_{\mathrm{eff}} &= \frac{A\phi}{\pi R^2}\int_0^{r_0} u \cdot 2\pi r \mathrm{d}r \\ &= -\frac{A\phi}{\pi R^2}\frac{\pi}{2\mu}\frac{v^4}{U^4}\frac{\mathrm{d}p}{\mathrm{d}x}\frac{{\mathrm{Re}_R}^4}{4}\left\{\frac{4\int_0^{r_0^*} r^*[r^* + \ln r^* + \gamma - \mathrm{Ei}(r^*)]\mathrm{d}r^*}{\frac{{\mathrm{Re}_R}^4}{4}} + 2\frac{{r_0^*}^2}{{\mathrm{Re}_R}^2}\right\}, \end{aligned} \tag{9}$$

where A and ϕ are the cross-section area and the porosity of the medium, respectively. Consequently, the effective permeability is $\kappa_{\mathrm{eff}} = \frac{\mu Q_{\mathrm{eff}}}{A(-\frac{\mathrm{d}p}{\mathrm{d}x})}$.

The intrinsic permeability, which depends only on microstructure of porous media within the Darcy flow regime, can be determined by the classical capillary model as $\kappa_{\mathrm{in}} = \frac{\mu Q_{\mathrm{Poi}}}{A(-\frac{\mathrm{d}p}{\mathrm{d}x})}$ with the volumetric flow rate for Poiseuille flow of capillaries, $Q_{\mathrm{Poi}} = -\frac{\pi}{2\mu}\frac{v^4}{U^4}\frac{\mathrm{d}p}{\mathrm{d}x}\frac{{\mathrm{Re}_R}^4}{4}\frac{A\phi}{\pi R^2}$. By comparing these two, the dimensionless permeability to characterize the inertia effect can be obtained as

$$\kappa^* = \frac{\kappa_{\mathrm{eff}}}{\kappa_{\mathrm{in}}} = \frac{4\int_0^{r_0^*} r^*[r^* + \ln r^* + \gamma - \mathrm{Ei}(r^*)]\mathrm{d}r^*}{\frac{{\mathrm{Re}_R}^4}{4}} + 2\frac{{r_0^*}^2}{{\mathrm{Re}_R}^2}. \tag{10}$$

Formula (10) indicates that the effective permeability decreases with Re_R, as Fig. 3 shows, which consists with the fact that the inertia effect reduces the effective permeability [43].

Results and discussion. Formula (10) is the exact solution, but not friendly enough to engineering applications. In this section, this Eq. (10) will be simplified and an approximated solution with a similar form as the quadratic equation will be theoretically obtained.

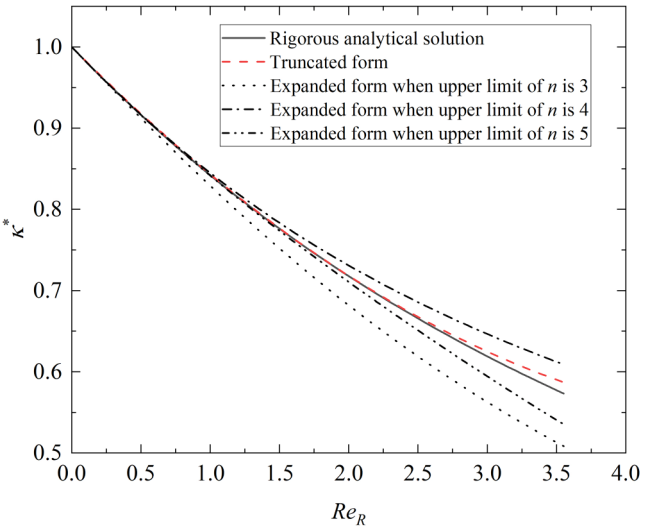

FIG. 3. The relationship between the ratio κ^* of the effective permeability to the intrinsic permeability and the Reynolds number Re_R. The expanded forms, formulas (14), (15), and (16), when the upper limit of n are 3, 4, 5 separately, gradually approach to the rigorous analytical result, formula (10). The truncated form (19) only slightly overestimates the analytical value.

a. Truncated form of analytical solution. The exponential integral in formula (10) can be expanded into different forms of infinite series and the Ramanujan's form is chosen for this study [46]:

$$\mathrm{Ei}(x) = \int_{-\infty}^{x} \frac{e^x}{x}\mathrm{d}x = \gamma + \ln x + e^{\frac{x}{2}} \sum_{n=1}^{\hat{n}} \frac{(-1)^{n-1}x^n}{n!2^{n-1}} \sum_{k=0}^{\lfloor (n-1)/2 \rfloor} \frac{1}{2k+1}. \tag{11}$$

Substitute formula (11) into formula (10). The permeability ratio at $\hat{n} = 3$ can be expressed as

$$\kappa^* = \left(\frac{r_0^*}{\mathrm{Re}_R}\right)^4 \left[2 + \frac{16}{3}\frac{1}{r_0^*} + e^{\frac{r_0^*}{2}}\left(-\frac{16}{9} + \frac{200}{9}\frac{1}{r_0^*} - \frac{496}{3}\frac{1}{r_0^{*2}} + \frac{1984}{3}\frac{1}{r_0^{*3}} - \frac{3968}{3}\frac{1}{r_0^{*4}}\right) + \frac{3968}{3}\frac{1}{r_0^{*4}}\right]. \tag{12}$$

It is further noticed that the exponential term, $e^{\frac{r_0^*}{2}}$, can be expanded into polynomial form by Taylor expansion

$$e^{\frac{r_0^*}{2}} = 1 + \sum_{N=1}^{\hat{N}} \frac{\left(\frac{r_0^*}{2}\right)^N}{N!}. \tag{13}$$

Truncation with $\hat{N} = 7$ of this expansion is enough for this work so that the simplified form of formula (12) is

$$\kappa^* = \left(\frac{r_0^*}{\mathrm{Re}_R}\right)^4 \left[2\left(\frac{\mathrm{Re}_R}{r_0^*}\right)^2 - 1 - \frac{8}{45}r_0^* - \frac{5}{108}r_0^{*2} - \frac{5}{504}r_0^{*3} - \frac{17}{12096}r_0^{*4} + \frac{1}{90720}r_0^{*5} - \frac{23}{725760}r_0^{*6} - \frac{1}{362880}r_0^{*7}\right]. \tag{14}$$

In the similar way, the truncated approximation at $\hat{n} = 4$:

$$\kappa^* = \left(\frac{r_0^*}{\mathrm{Re}_R}\right)^4 \left[2\left(\frac{\mathrm{Re}_R}{r_0^*}\right)^2 - 1 - \frac{8}{45}r_0^* - \frac{1}{36}r_0^{*2} + \frac{1}{720}r_0^{*3} - \frac{1}{8640}r_0^{*4} + \frac{7}{17280}r_0^{*5} - 2.89 \times 10^{-5} r_0^{*6} + \frac{1}{207360}r_0^{*7}\right], \tag{15}$$

that for $\hat{n} = 5$ is

$$\kappa^* = \left(\frac{r_0^*}{\mathrm{Re}_R}\right)^4 \left[2\left(\frac{\mathrm{Re}_R}{r_0^*}\right)^2 - 1 - \frac{8}{45}r_0^* - \frac{1}{36}r_0^{*2} - \frac{2}{525}r_0^{*3} - 2.71 \times 10^{-4} r_0^{*4} - \frac{487}{302400}r_0^{*5}\right]. \tag{16}$$

This process can be done so on and so forth for different values of $\hat{n}$, and it can be found that, from the truncated expressions (14), (15), and (16), the first four terms no longer change with values of $\hat{n}$. The higher order term than r_0^{*2} can be further negligible, and then we can get

$$\kappa^* = \left(\frac{r_0^*}{\mathrm{Re}_R}\right)^4 \left[2\left(\frac{\mathrm{Re}_R}{r_0^*}\right)^2 - 1 - \frac{8}{45}r_0^* - \frac{1}{36}r_0^{*2}\right]. \tag{17}$$

In this truncated approximation, the effective tube radius, r_0, is still unknown, which is the root of Eq. (8). Equation (8) is very hard to be solved analytically, but can be solved numerically so that the value of the ratio $\frac{r_0^*}{\mathrm{Re}_R}$ can be obtained by numerical fitting as

$$\frac{r_0^*}{\mathrm{Re}_R} = 0.0099{\mathrm{Re}_R}^2 - 0.1111\mathrm{Re}_R + 1. \tag{18}$$

Substituting formula (18) into formula (17) leads to a complex polynomial function of κ^* to Re_R. When Re_R is lower than ten, the high-order polynomial function can be simplified as a truncated quadratic form:

$$\kappa^* = 1 - 0.1727\mathrm{Re}_R + 0.0159{\mathrm{Re}_R}^2. \tag{19}$$

The comparison between the exact solution (10) with the approximation solutions, including the nth-order approximation (14), (15), (16), and the numerically truncated approximation (19) for κ^* is shown in Fig. 3. Within a limited value of Re_R (lower than 4 in the Fig. 3) the accuracy of approximations appears to increase with $\hat{n}$ when $\hat{n}$ is not higher than 5. It is good to find that the numerically truncated approximation agrees well with the exact analytical solution.

b. Recovery of the quadratic equation. Formula (19) gives an explicit approximation of the effective permeability reduced by inertia effects. The intrinsic permeability for the capillary model is $\kappa_{\mathrm{in}} = \frac{\phi R^2}{8}$, substitution of which into formula (19) leads to the empirical determination of κ_{eff} as

$$\kappa_{\mathrm{eff}} = \frac{\phi R^2}{8}\left(1 - 0.1727\mathrm{Re}_R + 0.0159{\mathrm{Re}_R}^2\right). \tag{20}$$

Substitution of this effective permeability into Darcy's law will bridge the pressure gradient with the Darcy velocity as

$$-\frac{\mathrm{d}p}{\mathrm{d}x} = \frac{8\mu}{\phi R^2}\frac{q}{1 - 0.1727\mathrm{Re}_R + 0.0159{\mathrm{Re}_R}^2}. \tag{21}$$

When Re_R is lower than ten, the value of $0.1727\mathrm{Re}_R - 0.0159{\mathrm{Re}_R}^2$ can be treated as a small number, Taylor expansions of $\frac{1}{1-x}$ may help to simplify further the relationship by

$$\frac{1}{1 - \left(0.1727\mathrm{Re}_R - 0.0159{\mathrm{Re}_R}^2\right)} = 1 + \sum_{N=1}^{\infty}\left(0.1727\mathrm{Re}_R - 0.0159{\mathrm{Re}_R}^2\right)^N, \tag{22}$$

so that the approximation becomes

$$-\frac{\mathrm{d}p}{\mathrm{d}x} = \frac{8\mu}{\phi R^2}q + \frac{1.3816}{\phi R}\rho q U - \frac{0.1272}{\phi \nu}\rho q U^2 + \cdots . \tag{23}$$

Note that in formula (23), U is the averaged streamwise velocity over the cross section of the capillary caused by inertia effects and q is the Darcy's velocity. The relationship between U and q, $U = q\frac{\phi}{1-\phi}$, is adopted in this work [47], which is consistent with the form of hydraulic diameter theory as indicate in (see the side bar titled The Reynolds Number for Porous Materials in [10]). This relationship also indicates that $M = \frac{\phi^2}{1-\phi}$ which is consistent with our previous assumption. Thus formula (23) becomes

$$-\frac{\mathrm{d}p}{\mathrm{d}x} = \frac{8\mu}{\phi R^2}q + \frac{1.3816}{(1-\phi)R}\rho q^2 - \frac{0.1272\phi}{(1-\phi)^2\nu}\rho q^3 + \cdots . \tag{24}$$

Equation (24) can be further truncated to the second order of the Darcy velocity when the velocity is not too high so that the quadratic equation is obtained:

$$-\frac{\mathrm{d}p}{\mathrm{d}x} = \frac{8\mu}{\phi R^2}q + \frac{1.3816}{(1-\phi)R}\rho q^2. \tag{25}$$

Thus, we obtain the quadratic approximation of the analytical solution of high-speed flow in porous media with inertia effects, which has a similar mathematical form as the Forchheimer equation but has no undefined or fitting parameters. Based on the derivation process, this equation is rigidly valid when Re_R is lower than 10, yet the suitability may expand far beyond as both positive and negative factors of high-order terms are neglected. The scope of this equation can be further clarified by comparisons with experimental data.

c. Validations by experimental data. To be compared with experimental data, Eq. (25) is reformed as

$$f = \frac{8}{\mathrm{Re}_R} + 1.3816, \tag{26}$$

where $\mathrm{Re}_R = \frac{qR}{\nu}\frac{\phi}{1-\phi}$ is the Reynolds number defined by U, $f = -\frac{\mathrm{d}p}{\mathrm{d}x}\frac{(1-\phi)R}{\rho q^2}$ is the friction factor as presented in [10,48]. The comparisons between Eq. (26) and the available experimental data from literature are shown in Fig. 4. In the experiments by [43], the fluid was water and the samples were packing of granular materials. The porosity ϕ, the Darcy velocity q and the pressure gradient $-\frac{\mathrm{d}p}{\mathrm{d}x}$ were given directly in experiments. The work of [43] provided the linear regime in table form which followed the Darcy's law for the numbers of test 1, 2, 4, 6, 8, 9, 16, and 19 among all 22 tests. By using these data, the intrinsic permeability can be determined as $\kappa_{\mathrm{in}} = \frac{\nu}{a'g}$, where g is gravity acceleration and a' is the constant for linear regime directly presented in [43]. The real tube radius in capillary model R is expressed as $R = \sqrt{\frac{8\kappa_{\mathrm{in}}}{\phi}} = \sqrt{\frac{8\nu}{\phi a' g}}$ by using these data. In experiments done by [44], the fluid was air and the samples were sintered metal particles. The experimental data of $\mathrm{Re}_\kappa = \frac{q\sqrt{\kappa_{\mathrm{in}}}}{\nu}$ and $f_\kappa = -\frac{\mathrm{d}p}{\mathrm{d}x}\frac{\sqrt{\kappa_{\mathrm{in}}}}{\rho q^2}$ were given. These data could be transformed as $\mathrm{Re}_R = \mathrm{Re}_\kappa\sqrt{\frac{8}{\phi}}\frac{\phi}{1-\phi}$, $f = f_\kappa(1-\phi)\sqrt{\frac{8}{\phi}}$. In experiments done by [45], the fluid was water and the samples were packing of steel balls. The results were presented in a $f_\kappa - \mathrm{Re}_\kappa$ form, whose definitions were the same. To validate our model, we plot all the experimental data together with the predictions by the Darcy's law and Eq. (26) in Fig. 4. We use log-log axes to cover the wide range of four to five orders of magnitude in both axes.

The results in Fig. 4 indicate that the flow resistance in porous media follows Darcy's law when the Reynolds number is lower than unity while is remarkably underestimated by the Darcy's law when Re_R is higher than unity. All the experimental data agrees with the predictions by Eq. (26) at the full range of Re_R, which proves that the new analytical solution and the empirical correlation can capture well the inertia effects of high-speed flows in porous media. It is interesting to find

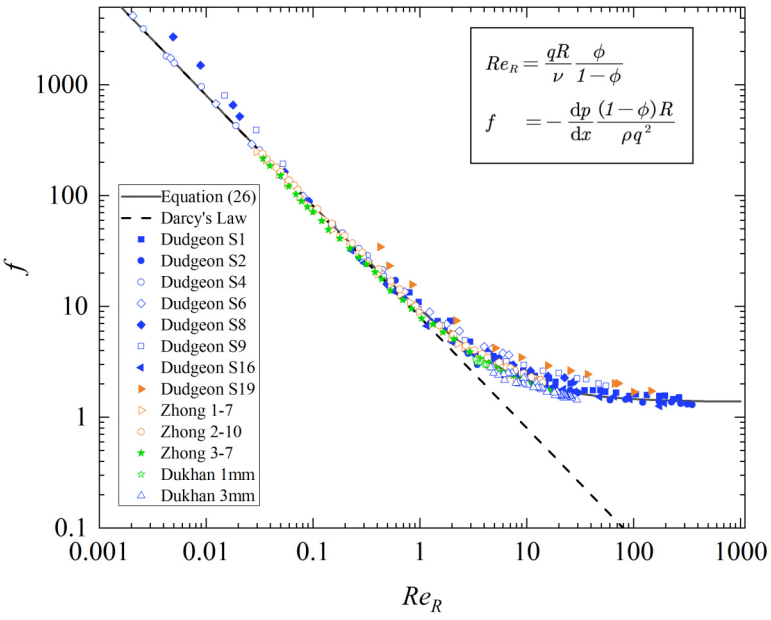

FIG. 4. The comparison of Eq. (26) with experimental data [43], [44], and [45]. The black dash line is the Darcy's law, whose form is $f = 8/\mathrm{Re}_R$. The definition of the horizontal and vertical axis is given as $\mathrm{Re}_R = \frac{qR}{\nu}\frac{\phi}{1-\phi}$, $f = -\frac{\mathrm{d}p}{\mathrm{d}x}\frac{(1-\phi)R}{\rho q^2}$. They are totally determined by experimentally measurable parameters, without any fitting parameter. The collected experimental data are plotted in different symbols.

that even though the theoretical derivation process is under the rigid condition of low values of Re_R ($\mathrm{Re}_R < 10$), the quadratic approximation works on a far wider range of Re_R (up to 10^3). This provides evidence for the reliability and validity of our model.

Conclusions. In this work, the inertia effect of high-speed flows through disordered porous media is analyzed at finite Reynolds numbers. An effective capillary model has been developed where the complex porous microstructure is modeled as a bundle of straight capillaries and the effective capillary radius is reduced by the secondary flow near walls at finite Re in porous media. Based on the effective capillary model, a new governing equation has been derived through considering the induced streamwise velocity by the secondary flows. The governing equation has a similar mathematical form as the classical Oseen equation for external flows, but works in this study to capture the inertia effects in the capillaries. Inspired by the asymptotic solution of flow through curved pipes in the previous study, the central-velocity boundary condition is adopted to obtain the analytical solution for the inertia effects with an integral form. To provide a friendly use empirical relationship for engineering applications, a truncated approximation has been deduced without any fitting parameters, which can recover the quadratic form as the Forchheimer equation for granular porous media. Our main novelty and originality, compared with other derivations, is that all constants in our expression, like 1.3816 in Eqs. (25) and (26), is strictly obtained, without any fitting from experimental data. The analytical solution and the truncated empirical correlation has been validated by the experimental data with a wide suitability.

Acknowledgments. This work is financially supported by the NSF grant of China (Grants No. U1837602, No. 12272207) and by the National Key R&D Program of China (Grant No. 2019YFA0708704).

[1] J. S. Andrade, U. M. S. Costa, M. P. Almeida, H. A. Makse, and H. E. Stanley, Inertial effects on fluid flow through disordered porous media, Phys. Rev. Lett. **82**, 5249 (1999).
[2] D. L. Koch and R. J. Hill, Inertial effects in suspension and porous-media flows, Annu. Rev. Fluid Mech. **33**, 619 (2001).
[3] A. Nissan and B. Berkowitz, Inertial effects on flow and transport in heterogeneous porous media, Phys. Rev. Lett. **120**, 054504 (2018).
[4] L. Germanou, M. T. Ho, Y. Zhang, and L. Wu, Shale gas permeability upscaling from the pore-scale, Phys. Fluids **32**, 102012 (2020).
[5] W. Lee, S. Yoon, and P. K. Kang, Inertia and diffusion effects on reactive transport with fluid-solid reactions in rough fracture flows, Phys. Rev. Fluids **8**, 054502 (2023).
[6] P. Forchheimer, Wasserbewegung durch boden, Z. Ver. Deutsch, Ing **45**, 1782 (1901).
[7] J. Bear, *Dynamics of Fluids in Porous Media* (Courier Corporation, New York, 2013).
[8] O. Reynolds, *Papers on Mechanical and Physical Subjects: 1881–1900* (Cambridge University Press, Cambridge, 1901).
[9] A. Dybbs and R. Edwards, A new look at porous media fluid mechanics–Darcy to turbulent, Fundam. Transp. Phenom. Porous Media **82**, 199 (1984).
[10] B. D. Wood, X. He, and V. Apte, Modeling turbulent flows in porous media, Annu. Rev. Fluid Mech. **52**, 171 (2020).
[11] S. Irmay, On the theoretical derivation of Darcy and Forchheimer formulas, EoS, Trans. Am. Geophys. Union **39**, 702 (1958).
[12] F. A. Dullien and M. I. Azzam, Flow rate-pressure gradient measurements in periodically nonuniform capillary tubes, AIChE J. **19**, 222 (1973).
[13] Y. Kaneda, The drag on a sparse random array of fixed spheres in flow at small but finite Reynolds number, J. Fluid Mech. **167**, 455 (1986).
[14] C. C. Mei and J. L. Auriault, The effect of weak inertia on flow through a porous medium, J. Fluid Mech. **222**, 647 (1991).
[15] T. Giorgi, Derivation of the Forchheimer law via matched asymptotic expansions, Transport Porous Med. **29**, 191 (1997).
[16] M. Hassanizadeh and W. G. Gray, General conservation equations for multi-phase systems: 1. Averaging procedure, Adv. Water Resour. **2**, 131 (1979).
[17] M. Hassanizadeh and W. G. Gray, General conservation equations for multi-phase systems: 2. Mass, momenta, energy, and entropy equations, Adv. Water Resour. **2**, 191 (1979).
[18] M. Hassanizadeh and W. G. Gray, General conservation equations for multi-phase systems: 3. Constitutive theory for porous media flow, Adv. Water Resour. **3**, 25 (1980).
[19] K. Vafai and C. L. Tien, Boundary and inertia effects on flow and heat transfer in porous media, Int. J. Heat Mass Transf. **24**, 195 (1981).
[20] M. Hassanizadeh and W. G. Gray, High velocity flow in porous media, Transp. Porous Med. **2**, 521 (1987).
[21] D. Ruth and H. Ma, On the derivation of the Forchheimer equation by means of the averaging theorem, Transp. Porous Med. **7**, 255 (1992).
[22] S. Whitaker, The forchheimer equation: A theoretical development, Transp. Porous Med. **25**, 27 (1996).
[23] D. Lasseux and F. J. Valdés-Parada, On the developments of Darcy's law to include inertial and slip effects, C.R. Mec. **345**, 660 (2017).
[24] L. Wu, M. T. Ho, L. Germanou, X. J. Gu, C. Liu, K. Xu, and Y. Zhang, On the apparent permeability of porous media in rarefied gas flows, J. Fluid Mech. **822**, 398 (2017).
[25] Z. Tian, D. Zhang, Y. Wang, G. Zhou, S. Zhang, and M. Wang, Inertial solution for high-pressure-difference pulse-decay measurement through microporous media, J. Fluid Mech. **971**, R1 (2023).
[26] W. Su, L. Gibelli, J. Li, M. K. Borg, and Y. Zhang, Kinetic modeling of nonequilibrium flow of hard-sphere dense gases, Phys. Rev. Fluids **8**, 013401 (2023).
[27] D. Lasseux, T. Zaouter, and F. J. Valdés-Parada, Determination of Klinkenberg and higher-order correction tensors for slip flow in porous media, Phys. Rev. Fluids **8**, 053401 (2023).
[28] F. Qiu, Y. Cai, Y. Zhou, J. Lu, and J. Hu, Thermodynamic characteristics of methane adsorption and desorption on varied rank coals a systematic study, Energy Fuels **38**, 269 (2024).

[29] R. J. Hill, D. L. Koch, and A. J. Ladd, The first effects of fluid inertia on flows in ordered and random arrays of spheres, J. Fluid Mech. **448**, 213 (2001).
[30] R. J. Hill, D. L. Koch, and A. J. Ladd, Moderate-Reynolds-number flows in ordered and random arrays of spheres, J. Fluid Mech. **448**, 243 (2001).
[31] M. Agnaou, D. Lasseux, and A. Ahmadi, Origin of the inertial deviation from Darcy's law: An investigation from a microscopic flow analysis on two-dimensional model structures, Phys. Rev. E **96**, 043105 (2017).
[32] H. Hasimoto, On the periodic fundamental solutions of the stokes equations and their application to viscous flow past a cubic array of spheres, J. Fluid Mech. **5**, 317 (1959).
[33] A. S. Sangani and A. Acrivos, Slow flow through a periodic array of spheres, Int. J. Multiphase Flow **8**, 343 (1982).
[34] A. Zick and G. Homsy, Stokes flow through periodic arrays of spheres, J. Fluid Mech. **115**, 13 (1982).
[35] R. Larson and J. Higdon, A periodic grain consolidation model of porous media, Phys. Fluids **1**, 38 (1989).
[36] M. Kaviany, *Principle of Heat Transfer in Porous Media* (Springer, New York, 1991).
[37] L. Klinkenberg, The permeability of porous media to liquids and gases, Drilling and Production Practice 200 (1941).
[38] W. R. Dean, Fluid motion in a curved channel, Proc. R. Soc. London A **121**, 402 (1928).
[39] F. Smith, Pulsatile flow in curved pipes, J. Fluid Mech. **71**, 15 (1975).
[40] S. Murata, Y. Miyake, and T. Inaba, Laminar flow in a curved pipe with varying curvature, J. Fluid Mech. **73**, 735 (1976).
[41] L. G. Leal, *Laminar Flow and Convective Transport Processes* (Cambridge University Press, Cambridge, 1992).
[42] C. W. Oseen, Uber die stokes' sche formel und uber eine verwandte aufgabe in der hydrodynamik, Arkiv Mat., Astron. och Fysik **6**, 1 (1910).
[43] C. Dudgeon, An experimental study of the flow of water through coarse granular media, La Houille Blanche **52**, 785 (1966).
[44] W. Zhong, X. Ji, C. Li, J. Fang, and F. Liu, Determination of permeability and inertial coefficients of sintered metal porous media using an isothermal chamber, Appl. Sci. **8**, 1670 (2018).
[45] N. Dukhan, O. Bağcı, and M. Özdemir, Experimental flow in various porous media and reconciliation of Forchheimer and Ergun relations, Exp. Therm Fluid Sci. **57**, 425 (2014).
[46] B. C. Berndt, *Ramanujan's Notebooks: Part IV* (Springer, Berlin, 1994), p. 130.
[47] A. E. Scheidegger, *The Physics of Flow through Porous Media* (University of Toronto Press, Toronto, 1957), pp. 141–144.
[48] R. B. Bird, Transport phenomena, Appl. Mech. Rev. **55**, R1 (2002).